4

5 **Geology and geochronology of the Tana Basin, Ethiopia: LIP volcanism, super**
6 **eruptions and Eocene-Oligocene environmental change**

7

8 A.R. Prave[1*], C.R. Bates[1], C.H. Donaldson[1], H. Toland[2], D.J. Condon[3], D. Mark[4], T.D. Raub[1]
9 [1]Department Earth and Environmental Sciences, University of St Andrews, KY16 9AL, UK
10 [2]Department Geography and Earth Sciences, Aberystwyth University, Wales, SY23 3DB
11 [3]NERC Isotope Geosciences Laboratory, BGS, Keyworth, NG12 5GG, UK
12 [4]Isotope Geoscience Unit, Scottish Universities Environmental Research Centre, East
13 Kilbride, G75 0QF, UK
14 *corresponding author: email ap13@st-andrews.ac.uk

15

16 **Abstract**

17 New geological and geochronological data define four episodes of volcanism for the Lake

18 Tana region in the northern Ethiopian portion of the Afro-Arabian Large Igneous

19 Province (LIP): pre-31 Ma flood basalt that yielded a single ^{40}Ar/^{39}Ar age of 34.05

20 ±0.54/0.56 Ma; thick and extensive felsic ignimbrites and rhyolites (minimum volume of

21 2-3 x 10^3 km^3) erupted between 31.108 ±0.020/0.041 Ma and 30.844 ±0.027/0.046 Ma

22 (U-Pb CA-ID-TIMS zircon ages); mafic volcanism bracketed by ^{40}Ar/^{39}Ar ages of 28.90

23 ±0.12/0.14 Ma and 23.75 ±0.02/0.04 Ma; and localised scoraceous basalt with an

24 ^{40}Ar/^{39}Ar age of 0.033 ±0.005/0.005 Ma. The felsic volcanism was the product of super

25 eruptions that created a 60-80 km diameter caldera marked by km-scale caldera-collapse

26 fault blocks and a steep-sided basin filled with a minimum of 180 m of sediment and the

27 present-day Lake Tana. These new data enable mapping, with a finer resolution than

28 previously possible, Afro-Arabian LIP volcanism onto the timeline of the Eocene-

29 Oligocene transition and show that neither the mafic nor silicic volcanism coincides

30 directly with perturbations in the geochemical records that span that transition. Our

31 results reinforce the view that it is not the development of a LIP alone but its rate of

32 effusion that contributes to inducing global-scale environmental change.

33

34 **Keywords:** LIP, Eocene-Oligocene transition, Lake Tana, flood basalt, super eruption

35

36 **1. Introduction**

37 Temporal coincidence between Large Igneous Provinces (LIPs) and worldwide

38 environmental perturbation is often considered evidence for causality (e.g. Bond &

39 Wignall 2014; Burgess et al. 2014), yet the Afro-Arabian LIP, estimated as 0.6–1.1M km^2

40   and 0.35–1.0 x 10⁶ km³ (Mohr and Zanettin 1988; Dessert et al. 2003), seemingly had

41   little influence on Cenozoic climate (Hofmann et al. 1997; Rochette et al. 1998; Ukstins

42   Peate et al. 2003). Here we present new geological and geochronological data that

43   provide a refined understanding of the development of that LIP and its temporal

44   relationship to the climatic events of the Eocene-Oligocene transition.

45

46   **1.1. Geological background.** The Ethiopian Highlands are a volcanic massif of flood and

47   shield volcano basalt 0.5 to 3 km thick that form spectacular trap topography (1500 to

48   4500 m altitudes) flanking the Main Ethiopian Rift (Fig. 1; Mohr 1983). Volcanic activity

49   was protracted but episodic: flood basalt at 31-29 Ma, shield volcanoes at 30-19 and 12-

50   10 Ma, felsic volcanism at 30-25, 20-15 and 12-3 Ma, and Pliocene-Quaternary basalt

51   (Hofmann et al. 1997; Pik et al. 1998; Rochette et al. 1998; Ayalew et al. 2002; Ukstins et

52   al. 2002; Coulié et al. 2003; Riisager et al. 2005). In the midst of the massif is a 16,500 km²

53   topographic depression that contains Lake Tana, the source of the Blue Nile and

54   Ethiopia's largest lake with a diameter of 60-80 km. The dominant rock type in the Tana

55   region is low-Ti tholeiitic Miocene-Pliocene basalt and lesser amounts of felsites and non-

56   marine sedimentary rocks and locally restricted basalt cinder cones and flows (Pik et al.

57   1998; Abate et al. 1998; Ayalew et al. 2002). Our petrological findings echo those of

58   previous workers and show that compositions are bimodal: sub- to mildly alkaline (MgO

59   5.0-9.5 wt%) olivine- to plagioclase-phyric basalt, and dacites to rhyolites including

60   banded finely crystalline to glassy rocks, crystal ± lithic ± vitric tuffs, obsidian-rich

61   agglomerates and coarse ignimbrites.

62

63   **2. Results: new geological data**

64   Our mapping defined five major units (Figs. 2 and 3). Flood basalt, with a base at ~700

65   m elevation and its top at ~1600 m. An overlying unit, many tens to several hundreds of

66   metres thick, of flow-banded rhyolite, pumice/lithic-rich and -poor tuffs, coarse-grained

67   silicic ignimbrites, volcanic breccias and epiclastic sandstone and agglomerate (Fig. 4);

68   clast sizes range from lapilli to bombs several metres in diameter. The felsic rocks occur

69   in fault blocks hundreds of metres in width, 0.2 to 3 km in length and arranged

70   centroclinally (dip generally inward) around the lake (Fig. 5a) although areas north and

71   east of the lake exhibit a more jumbled fault pattern relative to southern and western

72   areas. The fault blocks are present only within several tens of kilometres of Lake Tana

2

73   but the felsic rocks extend well beyond the map area.

74   The third unit ("Chilga beds" of Yemane et al. 1987) is patchily preserved, several

75   tens to at least two hundred metres thick, and consists of organic-rich to lignitic

76   mudstone and fine- to coarse-grained sandstone, thin felsic tuffs and silicite beds, and

77   interlayered sparsely olivine-phyric amygdaloidal (quartz- or calcite-filled) basalt and

78   andesitic basalt. The sedimentary rocks are lacustrine and fluvial deposits, and contain

79   fossil bone and plant material that, along with associated palynomorphs, indicate that

80   climate then was much wetter than today's (Yemane et al. 1987).

81   The fourth unit is olivine- and/or plagioclase-phyric and vesicle-rich to -poor basalt

82   that form 2-3 km high plateaux. Its base is an unconformity along which successive basalt

83   flows onlap and bury an irregular palaeotopography formed on the felsic fault blocks (Fig.

84   5b) and sedimentary-basalt unit ("Chilga beds"). Thick but variably developed kaolinite-

85   rich weathering profiles beneath the unconformity surface indicate a substantial hiatus

86   prior to the initial outpouring of the basalt forming the high plateaux. The fifth unit is

87   scoraceous basalt and cinder cones in areas south of Lake Tana.

88   Our geophysical surveys show that Lake Tana overlies a basin marked by sub-

89   vertical walls and filled with at least 180 m of flat-lying sediment (Fig. 6). The timing of

90   sedimentation remains to be determined but linear extrapolation using a ^{14}C age of ~17

91   ka obtained at 10.2 m depth in a 90 m core through those sediments (Marshall et al. 2011)

92   suggests that the base of the core is in excess of 150 ka. In effect, Tana is a steep-sided

93   bowl filled with thick flat-lying sediments whose ultimate age is unknown but predate

94   the scoraceous basalts that form the present-day dam and outflow of the lake.

95

96   **2.1. Caldera-forming super eruptions.** Previous workers interpreted the Tana basin as

97   a consequence of the confluence of three rift structures (e.g. Chorowicz et al. 1998). Our

98   new data suggest that it is a caldera: the centroclinal fault blocks decrease in magnitude

99   (over distances of tens of kilometres) away from the lake and pre-date the unconformably

100   overlying sedimentary-basalt ("Chilga beds") and plateaux-forming basalt units thus are

101   unrelated to the younger high-angle, largely dip-slip faults that transect all the rock units

102   in the Tana basin and which are part of the Neogene opening of the Main Ethiopia Rift.

103   Further, the ignimbrites and associated felsic rocks are thickest and coarsest adjacent to

104   Tana and thin and fine in all directions away from the lake. These rocks cover at least

105   10,000 km^2 but extend far beyond the map area and average 200-300 m in thickness

106 hence their minimum eruptive volume would have been 2000-3000 km³. These are

107 characteristics of super eruptions (e.g. Bryan and Ferrari 2013) and jointly with the

108 seismic data underpin our interpretation that Tana is a caldera ringed by fault blocks

109 formed by caldera collapse. Today's landscape reflects this ancient caldera exhumed by

110 head-ward erosion of the Blue Nile River system.

111

112 **3. Results: new geochronology data**

113 Our geochronology strategy was designed to constrain the timing of emplacement of the

114 felsic unit, determine the ages of the basalts bounding that unit and define the age of the

115 basalts that dam the outflow of the present-day lake (Figs. 2 and 3). Dates are shown with

116 two levels of uncertainty (±A/B) where A is the analytical uncertainty and B is the

117 analytical uncertainty combined with systematic uncertainties related to calibration and

118 decay constants; details of the samples, dating methodologies and analytical results can

119 be found in the Supplemental Files.

120   Age constraints for the felsic volcanism are from zircons separated from four

121 samples and analysed at the NERC Isotope Geoscience Laboratory, UK, using U-Pb

122 chemical abrasion-isotope dilution-thermal ionisation mass spectrometry (CA-ID-TIMS);

123 all samples were spiked using the gravimetrically calibrated ET535 or ET2535

124 EARTHTIME U-Pb tracer solutions (Condon et al. 2015; McLean et al. 2015; see

125 Supplemental Files). Constraints for the mafic volcanism are by $^{40}Ar/^{39}Ar$ analyses on

126 four samples done at the NERC Argon Isotope Facility, UK, following methods outlined in

127 Mark et al. 2010 (see Supplemental Files).

128

129 **3.1. Felsic samples.** Sample Hydro-1 is a lapilli tuff near the base of the felsite unit ~7

130 km southwest of Kunzla; four zircons were analysed and yield a mean age of 31.108

131 ±0.020/0.041 Ma. Sample Zege-1 is a flow-banded stony rhyolite in the central part of

132 the felsite unit exposed in an erosional window through Quaternary basalt ~7 km west

133 of Bahir Dar; four zircons were analysed and yield a mean age of 31.033 ±0.018/0.041

134 Ma. Samples Yifag-2 and Aby-1 are flow-banded feldspar-phyric rhyolites from the upper

135 part of the felsite unit ~1.5 and 1 km west of Yifag, respectively; five zircons from each

136 were analysed and yield mean ages of 30.858 ±0.024/0.044 Ma and 30.844 ±0.027/0.046

137 Ma, respectively.

138

3.2. Mafic samples. All mafic samples are olivine- and/or plagioclase-phyric basalt. Sample BNG1 was collected near the top of the lower flood basalt ~0.5 km southeast of the Blue Nile Falls and yielded a total fusion age of 34.05 ±0.54/0.56 Ma. Sample WD1 is from the sedimentary-basalt unit ~8 km west of Aykel and yielded a plateau age of 28.90 ±0.12/0.14 Ma. Sample KNZ1 is from the lower part of the upper basalt unit ~3 km south of Kunzla and yielded a plateau age of 23.75 ±0.02/0.04 Ma. Sample BHD1 is from the outflow of the Blue Nile River in Bahir Dar and yielded a plateau age of 0.033 ±0.005/0.005 Ma.

3.3. Geochronology summary. The new geochronology defines four distinct episodes of volcanism: (i) ~1 km thick flood basalt likely as old as ~34 Ma but of unknown duration; (ii) caldera-forming silicic super eruptions at ~31 Ma spanning ~250 kyr with a minimum erupted volume of 2000-3000 km^3; (iii) a second episode of mafic volcanism starting perhaps as early as ~29 Ma and extending to at least ~24 Ma; and (iv) localised basalt flows and cinder cones 33 ka in age. The 34 Ma age is older than the 31-29 Ma ages typically attributed to Ethiopian flood basalt (Hofmann et al. 1997; Rochette et al. 1998) and, even if that age is downplayed, this flood basalt can be no younger than the c. 31 Ma age of the overlying felsic rocks and hence older than most previously documented Afro-Arabian flood basalt. Determining if these phases are distinct requires further geochronology and mapping.

4. Discussion: Tana volcanism and Eocene-Oligocene environmental change

Stable isotope and organic geochemistry trends for the Cenozoic define one of the finest timelines of global change for anytime in Earth history (Fig. 7). Our new data permit a stricter evaluation than previously possible of Afro-Arabian LIP volcanism to those data.

4.1. Atmospheric CO_2 drawdown and C-O isotopes. Following a zenith of global warmth at ~55 Ma climate underwent a descent into the current state of bipolar icecaps (e.g. Zachos et al. 2001; Pälike et al 2006). The late Eocene-early Oligocene receives particular attention because of temporally distinct, sharp steps in C-O isotopes (~1-1.5‰, e.g. Oi1 and Oi-2 on Fig. 7; e.g. Miller et al. 1991; Coxall & Wilson 2011 and references therein) and declines in atmospheric CO_2 (~300-500 ppm; e.g. Zhang et al. 2013; Armstrong McKay et al. 2016 and references therein), each experiencing durations

5

172   estimated to be between several 10^4 and 10^5 years.

173   LIP emissions can generate global warming but can also cause global cooling due to

174   drawdown of those gases via weathering of fresh basalt. The Afro-Arabian LIP comprises

175   ~13% of today's exposed basalt but only accounts for ~4% of the annual flux of CO_2

176   drawdown because of its arid setting (Dessert et al. 2003). However, that region's climate

177   was much wetter during the Oligo-Miocene (e.g. Yemane et al. 1987) and, although no

178   quantitative estimates exist for how much wetter, the then rate of consumption of

179   atmospheric CO_2 of fresh basalt would have been higher than today's.

180   A back-of-the-envelope calculation can be undertaken to assess what the potential

181   effect of the Tana eruptions might have been on atmospheric CO_2 drawdown, and we

182   make two assumptions: (i) that the present-day preserved outcrop area of the Afro-

183   Arabian LIP approximates the original extent of flood basalt; and (ii) a flux of 4 x 10^{12}

184      $molCO_2$/year, representative of today's other low-latitude flood basalt provinces (Parana,

185   Deccan, Central American; Dessert et al. 2003), is a reasonable approximation for the

186   weathering of those basalts during Palaeogene time. The latter assumption is justifiable

187   because fossil evidence indicates relatively high precipitation during emplacement of the

188   Afro-Arabian LIP, which has 30-50% more surface area than those provinces. Further,

189   estimates of globally averaged CO_2 consumption by basalt weathering vary by ~4x, from

190   1.75 x 10^{13} $molCO_2$/year (Navarre-Stichler and Brantley 2007) to 4.08 x 10^{12}

191      $molCO_2$/year (Dessert et al. 2003) hence the chosen flux is a reasonable estimate.

192   Depending on estimates of atmospheric composition, 1 ppm of atmospheric CO_2 equates

193   to between ~3 to 7.8 Gt. Generating the stepwise decreases of 300-500 ppm CO_2 would

194   have required drawing down 2300-3900 Gt. Simplifying the calculation to focus solely on

195   weathering, a time-averaged flux of 4 x 10^{12} $molCO_2$/year would have drawn-down ~0.02

196      $GtCO_2$/year, requiring ~50-200 kyr to generate the estimated magnitude of change

197   indicated by each of the step-wise declines of CO_2. Volcanic degassing and/or cryptic

198   degassing (Armstrong Mckay et al. 2014) would have acted to reduce the declines but,

199   given the worldwide cooling trend at that time, that influence must have been minimal.

200   This thought experiment shows that a rate of weathering-induced CO_2 drawdown

201   can be obtained that is compatible with that implied by previous workers for the two

202   drops in Eocene-Oligocene CO_2. However, mapping our geochronological data onto the

203   timeline of Eocene-Oligocene environmental change (Fig. 7) refutes that possibility.

204   Assuming that (i) the c. 10^{4-5} year estimated durations required to drawdown CO_2 are

correct to within an order-of-magnitude and (ii) the absolute ages of those drawdowns based on the proxy records are broadly correct, then the c. 34 Ma episode of flood basalt predates by at least 0.5-1 Myr the proposed timing of the earlier drop in atmospheric CO_2 that began prior to the Eocene-Oligocene boundary (Fig. 7). Further, the second drop in CO_2 occurred ~3 Myr after the c. 29 Ma onset of the younger phase of mafic volcanism. The modelled pCO_2 data over that time are, within error, largely invariant for 3-4 Myr through the outpouring of the c. 34-31 Ma flood basalt and c. 31 Ma silicic eruptions, yet show a slight increase during the apparent gap in volcanic activity in the Tana region. Thus, there is a temporal disconnect between the timing of volcanic activity and the pattern of CO_2 fluctuations indicated by the proxy data records (Fig. 7). Although weathering of the Afro-Arabian basalts no doubt contributed to long-term CO_2 drawdown (e.g. Lefebvre et al. 2013; Kent & Muttoni 2013), our findings rule out volcanism as a key influence on the shorter-term, 10^{4-5} year draw-down timescales implied by the various CO_2 proxy data.

Our geochronology also reveals that there is no consistent relationship between the trend of O- and C-isotopes and the timing of mafic volcanism. O isotopes increase, and sharply so (i.e. at Oi-1, Fig. 7), entering the c. 34-31 Ma phase of volcanism but maintain a broadly invariant trend throughout that phase. In contrast, O-isotopes remain unperturbed across the initiation of the c. 29 Ma phase of mafic volcanism, reach a zenith (marked by Oi-2; Fig. 7) several millions of years after that onset, and then decline throughout the remaining phase of volcanic activity. We do not know the exact timing of onset of the pre-31 Ma flood basalt, and it is tempting to consider a possible link to the sharp increase in slope in O isotopes at the Eocene-Oligocene transition, but additional geochronology is needed to test this plausibility. The C-isotope profile also shows contrary relationships between volcanic episodes: C isotopes rise irregularly and then fall steadily through the c. 34-31 Ma phase of mafic volcanism, are unperturbed during the c. 31 Ma super eruptions, and rise irregularly through the c. 29-23 Ma phase of mafic volcanism. Thus, the c. 34-23 Myr span of Afro-Arabian LIP volcanism in the Tana region failed to imprint significantly on the isotopic compositions of the Eocene-Oligocene oceans and atmosphere.

4.2. Volatiles as kill mechanisms. The rate and magnitude of injection of sulphur and halogen molecules into the atmosphere from LIP volcanism has been highlighted as kill

238 mechanisms for mass extinction especially when devolitalisation of evaporite- and
239 organic-rich country rock occurs (e.g. Chenet et al. 2007; Svensen et al. 2009; Brand et al.
240 2012; Black et al. 2012). The Afro-Arabian LIP silicic volcanism released ~45 Gt S and
241 ~224 Gt Cl (Ayalew et al. 2002), in part attributable to volatiles derived from the 1-2 km
242 thick Mesozoic succession of which ~50% consists of marine carbonate and evaporite
243 rocks and minor lignites and coals (Wolela et al. 2008). No such estimates have been
244 made for the mafic volcanism, but a first-order approximation for the potential amount
245 of degassed volatiles from both the silicic and mafic lavas can be attempted. We make a
246 supposition that the amounts of S and Cl devolitalised by both types of volcanism scaled
247 proportionally to their respective volumes. The volume of basalt in the Afro-Arabian LIP
248 is ~6 x 10^4 km^3, which is 5-15x the total volume that has been estimated for felsic
249 volcanism across the entire LIP (0.3–1 x 10^6 km^3; Ukstins Peate et al. 2003). As such,
250 Afro-Arabian volcanism could have released 250 to 750 Gt S and 1300 to 3600 Gt Cl,
251 amounts that are comparable at order-of-magnitude uncertainties to those for other LIPs
252 such as the Deccan and Siberian traps (e.g. Black et al. 2012; Self et al. 2008). However,
253 Afro-Arabian volcanism postdates the c. 34–33.7 Ma acme of progressive/stepwise
254 plankton extinctions (Keller 2005; Pearson et al. 2008; Peters et al. 2013), which
255 highlights that, although the total halogen effusion of the Afro-Arabian LIP may have been
256 large enough to affect deleteriously the biosphere, the rate of effusion was below a
257 threshold necessary to cause major disruptions in ecosystems. A temporally calibrated
258 example is the Central Atlantic Magmatic Province where only the first (~600 kyr in
259 duration) of four volcanic pulses can be linked to an extinction event and the three later
260 pulses had little to no effect on the biosphere (Blackburn et al. 2013).

261

262 **4.3. Silicic super eruptions.** Our new data show that the Tana felsic eruptions were
263 comparable to some of the largest explosive volcanic events in Earth history. These
264 spanned 2-3 Myr as evident from ^{40}Ar/^{39}Ar plateau and single crystal ages and Rb-Sr
265 isochron ages on thick, widespread ignimbrites and tuffs elsewhere in Ethiopia, and on
266 correlative tephra layers 2700 km distant in the Indian Ocean (Baker et al. 1996; Coulié
267 et al. 2003; Ukstins Peate et al. 2003, 2008; Riisager et al. 2005). The timing of Oi-1 and
268 the c. 31 Ma super eruptions is interesting (Fig. 7) but similar spikes in O-isotopes occur
269 episodically through the Eocene-Oligocene, which urges caution and consideration of that
270 relationship as a coincidence rather than as a cause-and-effect, particularly given that the

271 O-isotope profile through the short interval of Tana super eruptions exhibits jagged rises
272 and falls not unlike those marking the several millions of years preceding and postdating
273 the super eruptions. As for the other isotopic proxies, they remain unperturbed by those
274 eruptions (Fig. 7). Perhaps this is unsurprising given that the mid-Oligocene eruption (c.
275 28 Ma) of the La Garita caldera that formed the Fish Canyon Tuff, the volumetrically
276 largest well-constrained silicic super eruption known for the Phanerozoic (e.g. Wotzlaw
277 et al. 2014), likewise does not coincide with a perturbation in the stable isotope data.
278

279 **5. Conclusion.** Mapping of our new age constraints onto the timeline for Eocene-
280 Oligocene environmental change reveals that there is neither a synchronicity in the
281 initiation of nor a consistency in the trend of the changes-in-slopes of marine isotopic
282 compositions and atmospheric CO_2 records from one volcanic event to another during
283 the Afro-Arabian LIP. This reconfirms that Afro-Arabian LIP volcanism was seemingly
284 ineffectual in causing significant deviation of the trajectory of climate change that had
285 begun in the early Palaeogene. Unlike the <1-2 Myr timescales documented for the
286 duration of other Phanerozoic LIPs, Afro-Arabian LIP volcanism was protracted and
287 lacked the necessary and sufficient rates of effusion and volatile emission to influence
288 global-scale environmental change. Further, assuming that the Tana super eruptions are
289 typical of those at other times in Earth history, our data imply that the role of super
290 eruptions in inducing Earth System change most likely has to be as part of an ensemble
291 of environmental circumstances rather than as a solo act.
292

300

301 **References**
302 Abate, B., Koeberl, C., Buchanan, P.C., Körner, W. 1998. Petrography and geochemistry of
303 basaltic and rhyodacitic rocks from Lake Tana and the Gimjabet-Kosober areas (North
304 Central Ethiopia). J. African Earth Sciences 26, 119-134.
305

306 Armstrong McKay, D.I., Tyrell, T., Wilson, P.A., Foster, G.L. 2014. Estimating the impact
307 of cryptic degassing of Large Igneous Provinces: a mid-Miocene case study. Earth and
308 Planetary Science Letters 403, 254-262.

310 Ayalew, D., Barbey, P., Marty, B., Reisberg, L., Yirgu, G., Pik, R. 2002. Source, genesis and
311 timing of giant ignimbrite deposits associated with Ethiopian continental flood basalts.
312 Geoch. Cosmoch. Acta 66, 1429-1448.

314 Baker, J., Snee, L., Menzies, M. 1996. A brief Oligocene period of flood volcanism in
315 Yemen: implications for the duration and rate of continental flood volcanism at the
316 Afro-Arabian triple junction. Earth and Planetary Science Letters 138, 39-55.

318 Black, B.A., Elkins-Tanton, L.T., Rowe, M.C., Ukstins Peate, I. 2012. Magnitude and
319 consequences of volatile release from the Siberian Traps. Earth and Planetary Science
320 Letters 317-318, 363-373.

322 Blackburn, T.J., Olsen, P.E., Bowring, S.A., McLean, N.M., Kent, D.V., Puffer, J., McHone, G.,
323 Rasbuty, E.T., Et-Touhami, M. 2013. Zircon U-Pb geochronology links the end-Triassic
324 Extinction with the Central Atlantic Magmatic Process. Science 340, 941-945.

326 Bond, D.P.G., Wignall, P.B. 2014. Large igneous provinces and mass extinctions an
327 update, in Keller, G. and Kerr, A.C., eds. Volcanism, Impacts, and Mass Extinctions:
328 Causes and Effects. Geol. Soc. Amer. Spec. Pap. 505, 29-55.

330 Brand, U., Pesenato, R., Came, R, Affek, H., Angiolini, L., Azmy, K., Farabegoli, E. 2012. The
331 end-Permian mass extinction: a rapid volcanic CO_2 and CH_4-climatic catastrophe.
332 Chemical Geology 322-323, 121-144.

334 Bryan, S.E., Ferrari, L. 2013. Large igneous provinces and silicic large igneous provinces:
335 progress in understanding over the last 25 years. Geol. Soc. Amer. Bull. 125, 1053-1078.

337 Burgess, S., Bowring, S., Shen, S-Z. 2014. High-precision timeline for Earth's most severe
338 extinction. Proceedings Nat. Acad. Sci. USA. 111, 3316-3321.

340 Chenet, A.L., Quidelleur, X., Fluteau, F., Courtillot, V., Bajpal, S. 2007. [40]K-[40]Ar dating of
341 the main Deccan large igneous province: further evidence of KTB age and short
342 duration. Earth Planet. Sci. Lett. 263, 1-15.

344 Condon, D. J., Schoene, B., McLean, N., Bowring, S. A., Parrish, R. 2015. Metrology and
345 traceability of U-Pb isotope dilution geochronology (EARTHTIME Tracer Calibration
346 Part I): Geochimica et Cosmochimica Acta, doi:10.1016/j.gca.2015.05.026

348 Chorowicz, J., Collet, B., Bonavia, F.F., Mohr, P., Parrot, J.F., Korme, T. 1998. The Tana
349 basin, Ethiopia: intra-plateau uplift, rifting and subsidence. Tectonophys. 295, 351-367.

351 Coulié, E., Quidelleur, X., Gillot, P-Y., Courtillot, V., Lefèvre, J-C., Chiesa, S. 2003.
352 Comparative K-Ar and Ar/Ar dating of Ethiopian and Yemenite Oligocene volcanism:
353 implications for timing and duration of the Ethiopian traps. Earth and Planetary Science
354 Letters 206, 477-492.

355

356 Coxall, H.K., Wilson, P.A., Pälike, H., Lear, C.H., Backman, J. 2005. Rapid stepwise onset of
357 Antarctic glaciation and deeper calcite compensation depth in the Pacific Ocean. Nature
358 433, 53-57.

359

360 Cramer, B.S., Toggweiler, J.R., Wright, J.D., Katz, M.E., Miller, K.G. 2009. Ocean
361 overturning since the Late Cretaceous: inferences from a new benthic foraminiferal
362 isotope compilation. Paleoceanography 24, doi:10.1029/2008PA001683.

363

364 Dessert, C., Depré, B., Gaillardet, J., François, L.M., Allègre, C. 2003. Basalt weathering
365 laws and impact of basalt weathering on the global carbon cycle. Chem. Geol. 202, 257-
366 273.

367

368 Hofmann, C., Courtillot, V., Féraud, G., Rochette, P., Yirgu, G., Ketefo, E., Pik, R. 1997.
369 Timing of the Ethiopian flood basalt event and implications for plume birth and global
370 change. Nature 389, 838-841.

371

372 Keller, G. 2005. Impacts, volcanism and mass extinction: random coincidence or cause
373 and effect. Australian J. Earth Sci. 52, 725-757.

374

375 Kent, D.V., Muttoni, G. 2013. Modulation of Late Cretaceous and Cenozoic climate by
376 variable drawdown of atmospheric pCO$_2$ from weathering of basaltic provinces on
377 continents drifting through the equatorial humid belt. Clim. Past 9, 524-546.

378

379 Lefebvre, V., Donnadieu, Y., Godderis, Y., Fluteau, F., Hubert-Theuo, F. 2013. Was the
380 Antarctic deglaciation caused by a high degassing rate during the early Cenozoic. Earth
381 and Planetary Science Letters 371-372, 203-211.

382

383 Mark, D.F., Gonzalez, S., Huddart, D., Bohnel, H. 2010. Dating of the Valsequillo volcanic
384 deposits: Resolution of an ongoing controversy in Central Mexico. Journal of Human
385 Evolution 58, 441-445.

386

387 Marshall, M.H., Lamb, H.F., Huws, D., Davies, S.J., Bates, R., Bloemendal, J., Boyle, J., Leng,
388 M.J., Umer, M., Bryant, C. 2011. Late Pleistocene and Holocene drought events at Lake
389 Tana, the source of the Blue Nile. Global and Planetary Change 78, 147-161.

390

391 McLean, N., Condon, D.J., Schoene, B., Bowring, S.A. 2015. Evaluating uncertainties in the
392 calibration of isotopic reference materials and multi-element isotopic tracers
393 (EARTHTIME Tracer Calibration Part II): Geochimica et Cosmochimica Acta,
394 doi:10.1016/j.gca.2015.02.040

395

396 Miller, K.G., Wright, J.D., Fairbanks, R.G. 1991. Unlocking the Ice House: Oligocene–
397 Miocene oxygen isotopes, eustasy, and margin erosion. J. Geophys. Res. 96, 6829–6848.

398

399 Mohr, P. 1983. Ethiopian flood basalt province. Nature 303, 577-584.

400

401 Mohr, P., Zanettin, B. 1988. The Ethiopian flood basalt province, in. J.D. Macdougall (Ed)
402 Continental Flood Basalts. Kluwer, Dordrecht, 63-110.

403

404   Navarre-Sitchler, A., Brantley, S. 2007. Basalt weathering across scales. Earth Planet. Sci.
405   Lett. 261, 321-334.
406
407   Pälike, H., Norris, R.D., Herrle, J.O., Wilson, P.A., Coxall, H.K., Lear, C.H., Shackleton, N.J.,
408   Triparti, A.K., Wade, B.S. 2006. The heartbeat of the Oligocene climate system. Science
409   324, 1894-1898.
410
411   Pagani, M., Huber, M., Liu, Z., Bohaty, S.M., Henderiks, J., Sijp, W., Krishnan, S., DeConto,
412   R.M. 2011. The role of carbon dioxide during onset of Antarctic glaciation. Science 334,
413   1261-1264.
414
415   Pearson, P.N., McMillan, I.K., Wade, B.S., Jones, T.D., Coxall, H.K., Brown, P.R., Lear, C.H.
416   2008. Extinction and environmental change across the Eocene-Oligocene boundary in
417   Tanzania. Geology 36, 179-182.
418
419   Peters, S.E., Kelly, D.C., Fraass, J. 2013. Oceanographic controls on the diversity and
420   extinction of planktonic foraminifera. Nature 493, 398-01.
421
422   Pik, R., Deniel, C, Coulon, C, Yirgu, G., Hofmann, Ayalew, D. 1998. The northwestern
423   Ethiopian Plateau flood basalts: classification and spatial distribution of magma types. J.
424   Volcanology and Geothermal Research 81, 91-111.
425
426   Pik, R., Deniel, C, Coulon, C, Yirgu, Marty, B. 1999. Isotopic and trace element signatures
427   of Ethiopian flood basalts: evidence for plume-lithosphere interactions. Geochim.
428   Cosmoch. Acta 63, 2263-2279.
429
430   Riisager, P., Knight, K.B., Baker, J.A., Ukstins Peate, I., Al-Kasadi, M., Al-Subbary, A.,
431   Renne, P.R. 2005. Paleomagnetism and 40Ar/39Ar geochronology of Yemeni Oligocene
432   volcanics: implications for timing and duration of Afro-Arabian traps and geometry of
433   the Oligocene paleomagnetic field. Earth Planet. Sci. Lett. 237, 647-672.
434
435   Rochette, P., Tamrat, E., Féraud, Pik, R., Courtillot, V., Ketefo, E., Coulon, C., Hoffmann, C.,
436   Vandamme, D., Yirgu, G. 1998. Magnetostratigraphy and timing of the Oligocene
437   Ethiopian traps. Earth Planet. Sci. Lett. 164, 497-510.
438
439   Self, S., Blake, S., Sharma, K., Widdowson, M., Sephton, S. 2008. Sulfur and chlorine in
440   Late Cretaceous Deccan magmas and eruptive gas release. Science 319, 1654-1657.
441
442   Svensen, H., Planke, S., Polozov, A.G., Schmidbauer, N., Corfu, F., Podladchikov, Y.Y.,
443   Jamveit, B. 2009. Siberian gas venting and the end Permian mass extinction. Earth and
444   Planetary Science Letters 277, 490-500.
445
446   Ukstins, I.A., Renne, P.R., Wolfenden, E., Baker, J., Ayalew, D., Menzies, M. 2002. Matching
447   conjugate volcanic rifted margins: [40]Ar/[39]Ar chronostratigraphy of pre- and syn-rift
448   bimodal flood volcanism in Ethiopia and Yemen. Earth Planet. Sci. Lett. 198, 289-306.
449
450   Ukstins Peate, I., Baker, J.A., Kent, A.J.R., Al-Kadasi, M., Al-Subbary, A., Ayalew, D.,
451   Menzies, M. 2003. Correlation of Indian Ocean tephra to individual Oligocene silicic
452   eruptions from the Afro-Arabian flood volcanism. Earth Planet. Sci. Lett. 211, 311-327.

453

454 Ukstins Peate, I., Kent, A.J.R., Baker, J.A., Menzies, M.A. 2008. Extreme geochemical
455 heterogeneity in Afro-Arabian Oligocene tephras: preserving fractional crystallization
456 and mafic recharge processes in silicic magma chambers. Lithos 102, 260-278.

457

458 Westerhold, T., Rohl, U., Palike, H., Wilkens, R., Wilson, P.A., Acton, G. 2014. Orbitally
459 tuned timescale and astronomical forcing in the middle Eocene to early Oligocene.
460 Climate of the Past 10, 955-973.

461

462 Wolela, A. 2008. Sedimentation of the Triassic-Jurassic Adrigat Sandstone Formation,
463 Blue Nile (Abay) Basin, Ethiopia. J. Afr. Earth Sci. 52, 30-42.

464

465 Wotzlaw, J-F., Schalteger, U., Frick, D.A., Dungan, M.A., Gerdes, A., Günther. 2014.
466 Tracking the evolution of large-volume silicic magma reservoirs from assembly to
467 supereruption. Geology 41, 867-870.

468

469 Yemane, K., Robert, C., Bonnefille, R. 1987. Pollen and clay mineral assemblages of a late
470 Miocene lacustrine sequence from the Northwestern Ethiopian Highlands.
471 Palaeogeography, Palaeoclimatology, Palaeoecology 60, 123-141.

472

473 Zachos, J.C., Dickens, G.R., Zeebe, R.E. 2008. An early Cenozoic perspective on
474 greenhouse warming and carbon-cycle dynamics. Nature 451, 279-283.

475

476 Zachos, J.C., Pagani, M., Sloan, L., Thomas, E., Billups, K. 2001. Global climate 65 Ma to
477 Present. Science 292, 686-693.

478

479 Zhang, Y.G., Pagani, M, Liu, Z., Bohaty, S.M., DeConto, R. 2013. A 40-million-year history
480 of atmospheric CO_2. Philos. Trans. Roy. Soc A, 1-20.

481
482

Figure 1. Generalised Cenozoic geology of the regions bordering the Main Ethiopian Rift system (simplified from the Geological Map of Ethiopia). Circled 'A' is the location of Addis Ababa.

Figure 2. Simplified geological map of the Lake Tana region based on mapping done during this work.
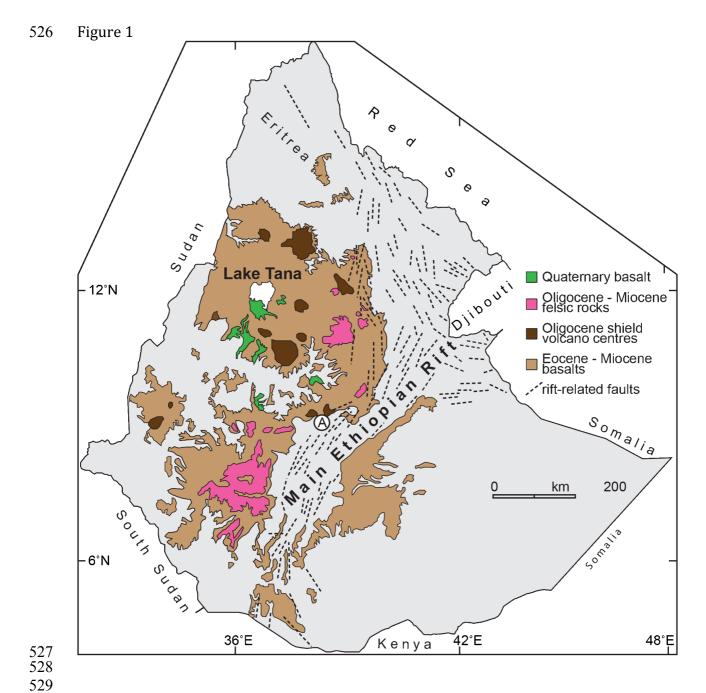
Figure 3. Stratigraphy of the Lake Tana region showing the four map units and position of geochronology samples. See text for details and Supplementary Files for GPS locations of samples. m.a.s.l. – metres above sea level.

Figure 4. Felsic volcanic rocks. **A.** Rhyolite domes 10-20 km southeast of Kunzla (southwest corner of Lake Tana). **B.** Tilted rhyolite dome 5 km west of Gorgora (north-central margin of Lake Tana); basal part consists of flow-banded rhyolite whereas inner part of dome consists of more massive rhyolite. **C.** Flow-banded rhyolite of sample Aby-1 (northeast corner of Lake Tana) that yielded a U-Pb zircon age of 30.844 ±0.027/0.046 Ma. **D and E.** Massive ignimbrite flows and large bomb of pumiceous and banded rhyolite (~12 km west of Yifag, northeast margin of Lake Tana). **F and G.** Fragmental texture of ignimbrite deposits; F contains a variety of felsic clasts and minor mafic clasts whereas G is mostly pumice (area west of Gorgora, north-central shoreline of Lake Tana). **H.** Cross-bedded volcaniclastic conglomerate-sandstone with obsidian and felsic volcanic clasts and rare basalt clasts; this unit overlies sharply the felsic tuff of sample Hydro-1 (15 km southwest of Kunzla) that yielded a U-Pb zircon age of 31.108 ±0.020/0.041 Ma.
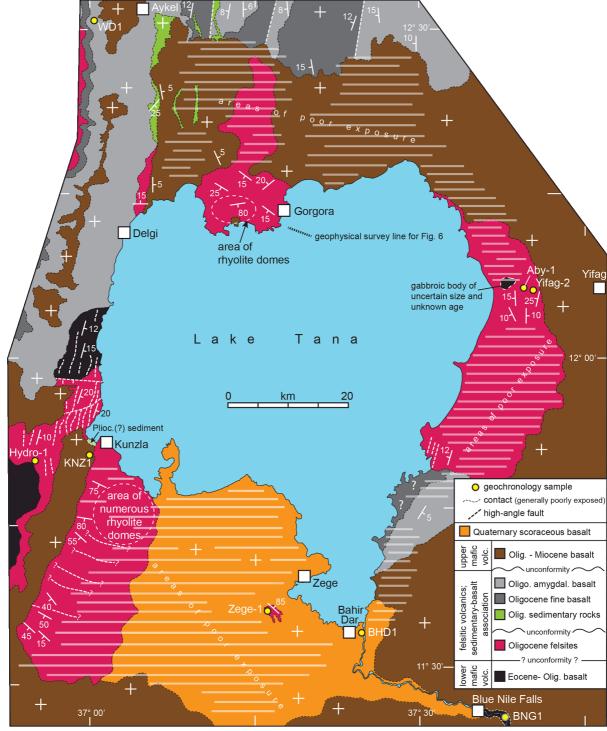
Figure 5. Structural features of the felsic unit. **A.** East-tilted fault blocks of silicic ignimbrite and tuff (~5 km northwest of Kunzla, southwest margin of Lake Tana). **B.** Progressive onlap and burial of c. 31 Ma southwest-tilted felsitic rocks by flat-lying c. 24 Ma basalt (~20 km south of Kunzla).
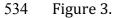
Figure 6. Seismic profile showing steep-sided bedrock margin beneath Lake Tana and how the sedimentary fill abuts against and buries those margins. The sediments are >180m thick (and likely much thicker) and linear extrapolation of the ^{14}C age for the topmost desiccation surface (Marshall et al. 2011) would imply that the base of the seismically imaged sediment is in excess of 150 ka.

Figure 7. Isotopic and atmospheric CO_2 envelopes for the Cenozoic; grey and black shading denotes age brackets for volcanism in the Lake Tana and surrounding regions. C- and O-isotope envelopes are from Zachos et al. (2001, 2008) and other proposed best-fit solid lines are from Cramer et al. (2009). CO_2 trends generalised from multiple proxies as reported by Pagani et al. (2011) and Zhang et al. (2013). Timescale calibration follows Westerhold et al. (2014). Oi and Mi: oxygen isotope events.
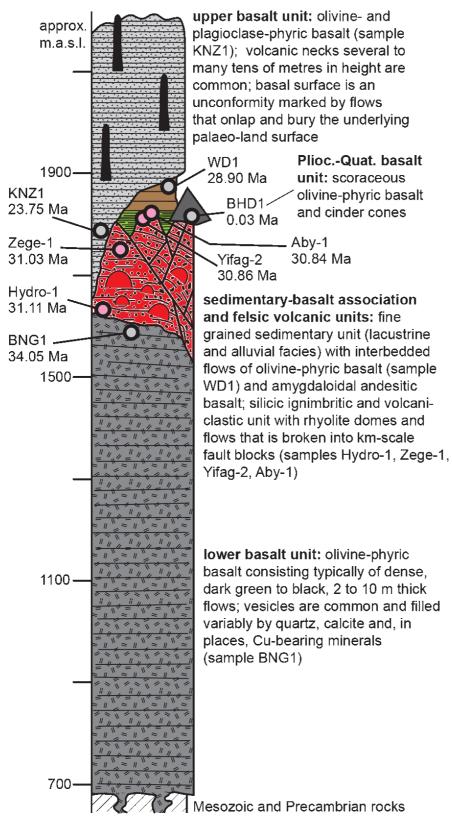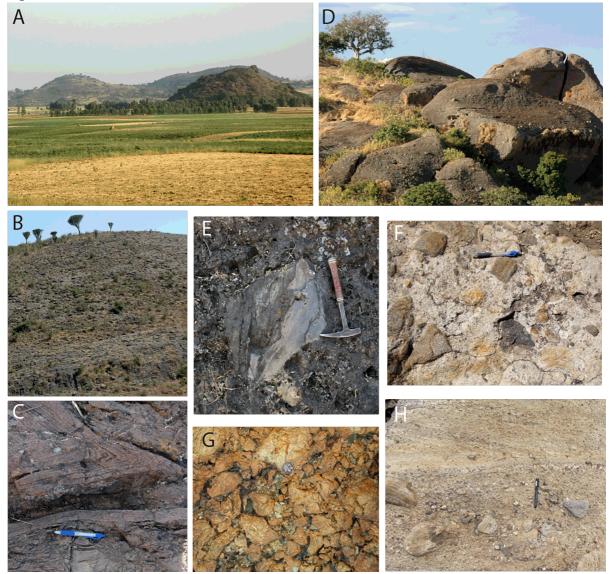
526   Figure 1

530   Figure 2.

531
532
533

534   Figure 3.

Lake Tana region stratigraphy

upper basalt unit: olivine- and plagioclase-phyric basalt (sample KNZ1); volcanic necks several to many tens of metres in height are common; basal surface is an unconformity marked by flows that onlap and bury the underlying palaeo-land surface

approx. m.a.s.l.

1900

KNZ1
23.75 Ma

Zege-1
31.03 Ma

Hydro-1
31.11 Ma

BNG1
34.05 Ma

1500

1100

700

WD1
28.90 Ma

BHD1
0.03 Ma

Aby-1
30.84 Ma

Yifag-2
30.86 Ma

Plioc.-Quat. basalt unit: scoraceous olivine-phyric basalt and cinder cones

sedimentary-basalt association and felsic volcanic units: fine grained sedimentary unit (lacustrine and alluvial facies) with interbedded flows of olivine-phyric basalt (sample WD1) and amygdaloidal andesitic basalt; silicic ignimbritic and volcani-clastic unit with rhyolite domes and flows that is broken into km-scale fault blocks (samples Hydro-1, Zege-1, Yifag-2, Aby-1)

lower basalt unit: olivine-phyric basalt consisting typically of dense, dark green to black, 2 to 10 m thick flows; vesicles are common and filled variably by quartz, calcite and, in places, Cu-bearing minerals (sample BNG1)
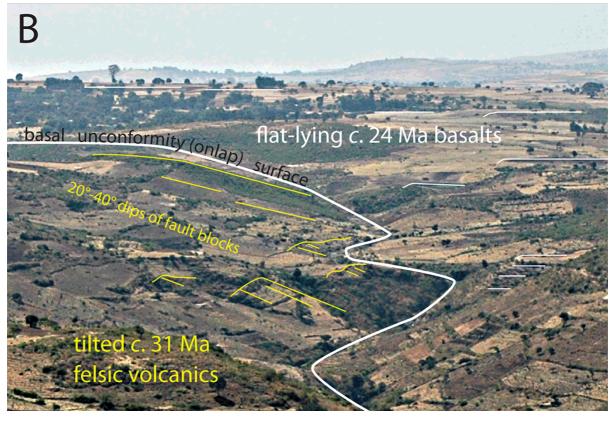
Mesozoic and Precambrian rocks

535
536
537

17

538   Figure 4.

542   Figure 5.

546   Figure 6.

547
548
549

Figure 7.